An accurate method for predicting spatial variability of maize yield from UAV-based plant height estimation: a tool for monitoring agronomic field experiments

Jean-Marc Gilliot, Joël Michelin, Dalila Hadjar, Sabine Houot

An accurate method for predicting spatial variability of maize yield from UAV-based plant height estimation: a tool for monitoring agronomic field experiments

J.M. Gilliot[a]*, J. Michelin[a], D. Hadjard[a], S. Houot[a]

[a]UMR ECOSYS, INRAE, AgroParisTech, Université Paris-Saclay, 78850, Thiverval-Grignon, France.

*Corresponding author: jean-marc.gilliot@agroparistech.fr

Tel: (33) 1-30-81-52-71 Fax: (33) 1-30-81-53-96

Author version

Published in
Precision Agriculture
An International Journal on Advances in Precision Agriculture
ISSN 1385-2256 Volume 22 Number 3 Precision Agric (2021) 22:897-921
DOI 10.1007/s11119-020-09764-w

Abstract

Estimating aboveground biomass is important for monitoring crop growth in agronomic field experiments. Often this estimation is done manually, destructively (mowing) or not (counting) on a relatively limited number of sub-plots within an experiment. In the presence of spatial heterogeneity in experiment fields, sensors developed for precision agriculture, have shown great potential to automate this estimation efficiently and provide a spatially continuous measurement over an entire plot. This study investigated the suitability of using an unmanned aerial vehicle (UAV) for biomass and yield estimations in an agronomic field experiment. The main objectives of this work were to compare the estimates made from manual field sampling with those made from UAV data and finally to calculate the improvement that can be expected from the use of UAVs. A 6-ha maize field was studied, with plot treatments for the study of the exogenous organic matter (EOM) amendment effect on crop development. 3D surface models were created from high resolution UAV RGB imagery, before crop emergence and during crop development. The difference between both surface models resulted in crop height which was evaluated against 38 reference points with an R^2 of 0.9 and prediction error of 0.16 m. Regression models were used to predict above-ground biomass and grain yield (fresh or dry). Dried grain yield prediction with a generalized additive model gave an error of 0.8 t ha^{-1} calculated on 100 in-field validation measurements, corresponding to a relative error of 14.77 %. UAV-based yield estimates from dry biomass were 15% more accurate than manual yield estimation.

Keywords Unmanned Aerial Vehicle (UAV) . Crop Surface Model (CSM) . Yield prediction . Photogrammetry . Biomass estimation

Introduction

Precision agriculture (PA) can help to meet the challenge of feeding an increasing population by optimizing the use of crop inputs towards a low-input sustainable agriculture (Zhang et al. 2002; Lindblom et al. 2017). Quantitative estimation of crop vegetative development and health is a major step in determining both the types of interventions and doses of products during crop operations such as fertilization or phytosanitary treatments and for yield prediction. Improvements in crop management related to PA are based on measuring and managing within-field variability of crop development. These measurements have been made possible using global navigation satellite systems (GNSS) and various sensors to exhaustively quantify the current biomass level at each location in the plot, in a non-destructive manner. Godwin and Miller (2003) proposed four major categories of field factors influencing spatial variations of yield: (i) soil water content, (ii) topography and micro-climate, (iii) soil nutrition and (iv) weeds, pests and diseases. Many sensors have been designed to map those factors as well as crop biomass. Ground-based sensors, mounted on a tractor or other land vehicle, provide information "on the go" (Barnes et al. 2003). In other cases, the sensors are installed on satellites or aircraft, but more recently with the increased miniaturization of sensors also on UAVs (Mulla 2013). The main advantages of UAV for PA are: a very high spatial and temporal resolution, a low utilization cost and an easily programmed image acquisition (Zhang and Kovacs 2012). UAV imagery have been successfully used for monitoring various crops, such as wheat (Duan et al. 2017), barley (Bendig et al. 2015), rapeseed (Verger et al. 2014), maize (Castaldi et al. 2017) and rice (Zhou et al. 2017). An increasing variety of sensors are used on-board UAVs for agricultural applications. Some professional aerial metric cameras have been adapted to UAV such as the IGN Lightweight Camera (IGN Lightweight Camera, IGN, Saint-Mandé, France) (IGN 2016) or the iXM-100 Phase One aerial camera (iXM-100, Phase one, Copenhagen, Denmark) (Phase one 2018). Despite their performance, they have not been used widely due to their high cost. Many studies have shown that quite acceptable results can be achieved with standard non-metric RGB digital cameras (Johnson et al. 2003; Poblete-Echeverría et al. 2017). As the near infrared spectral range is very interesting especially for monitoring plant biomass, some authors use professional multispectral or hyperspectral cameras. However, these cameras have a much lower resolution than RGB cameras and are much more expensive. For accurate 3D data acquisition, active LiDAR (light detection and ranging) sensors have been integrated on UAVs, such as the Riegl VUX-1UAV (VUX-1UAV, Riegl, Horn, Austria), Velodyne HDL-32E scanner (HDL-32E, Velodyne, San Jose, USA) or YellowScan (Vx-20, YellowScan, Montferrier sur Lez, France) (Eitel et al. 2016). Concerning UAV platforms, two main categories are commonly used: (i) fixed wing aircrafts, that are generally lightweight and therefore can only carry light sensors, but with a relatively long flight time (from 30 to 45 minutes); (ii) rotary wing UAV, which are of helicopter type, also called multirotor, which provide a great stability of flight, but also shorter flight times. Information on crop development has traditionally been studied by satellite-based sensor systems (Pinter et al. 2003). Aboveground biomass, leaf area index (LAI) and chlorophyll content can be estimated accurately from reflectance information and vegetation indices (VIs). Since similar sensors now exist for UAVs, the methods have been adapted for UAVs (Hunt et al. 2010; Verger et al. 2014; Duan et al. 2017). Similarly, 3D reconstruction from stereo images has been efficiently adapted to crop monitoring since 2009 through very high resolution of UAV imagery (Eisenbeiss 2009). 3D surface reconstruction produces a digital surface model (DSM), which is a digital representation of surface topography, including crops on the ground; it is also called a crop surface model (CSM) (Bendig 2015). Crop height is commonly used for assessing in-field crop

development (Catchpole and Wheeler 1992; Ganguli et al. 2000). Two main technologies may be used to acquire a CSM: (i) LiDAR and (ii) photogrammetry. Terrestrial laser scanning (TLS) was first used to create CSMs (Hoffmeister et al. 2010; Liu et al. 2017; Sun et al. 2017). UAV photogrammetry is an inexpensive alternative to LiDAR, as it only requires a good quality RGB camera and the UAV (Hugenholtz et al. 2013). For example, Bendig et al. (2014) estimated barley biomass from multi-temporal CSMs over one growing season, Li et al. (2016) predicted maize height from low-cost UAV images with an accuracy of 0.11 m, Holman et al. (2016) used photogrammetry as a new standard for high-throughput phenotyping of crop heights and Hassan et al. (2019) studied growth dynamics in bread wheat.

In this study, the main objective was to evaluate the benefits of high spatial resolution of crop development derived from UAV RGB imagery versus manual estimation on the ground from a limited number of sub-plots, for monitoring field agronomic experiments. The approach was based on the calculation of the difference of two DSMs created from separate UAV flights: one when vegetation is present, and one over bare soil to capture the field topography. The specific objectives were to: (i) determine how accurately plant height can be estimated by UAV photogrammetry; (ii) evaluate the quality of maize yield prediction from plant height measurements; (iii) assess whether it would be possible to replace the UAV flight over bare soil with DSM available from topographical data providers; (iv) compare manual and UAV CSM-based yield predictions. The hypothesis of the study was that yield estimation in the different plots of an agronomic experiment is more reliable using a UAV than a series of manual measurements that are extrapolated.

Material and methods

Study area

In 1998, the QualiAgro long-term experiment (Inrae 2019) was started within a collaboration between the National Research Institute for Agriculture, food and Environment (INRAE) and Veolia Environment Research and Innovation. The main objectives of this experiment were to study the effect of repeated applications of exogenous organic matter (EOM) on crop development and their impacts on soil and water (Noirot-Cosson et al. 2016). This 6-ha field is located at Feucherolles in the Paris region, France (48.8965° N, 1.975° E). It is divided into 40 plots (each of 10 m x 45 m) (Fig. 1) organized in four repetition blocks. Four EOM have been studied: a farmyard manure (FYM), a municipal solid waste compost (MSW), a biowaste compost (BIO) and a co-compost of green waste and sewage sludge (GWS). The effects of the EOM were compared to control plots (CTR) that do not receive any EOM input. Finally, half of the plots received a minimal additional mineral N dose, while the other half of the plots received an optimal one. The study was conducted in 2014, when the field was sown with maize on April 22/23, by a Pioneer PR39F58 (Pioneer PR39F58, Pioneer semences, Aussonne, France), with a 6-row seed drill (row spacing 0.8 m) and a density between 92000 and 95000 seeds ha^{-1}. No pesticides were applied during the crop growth.

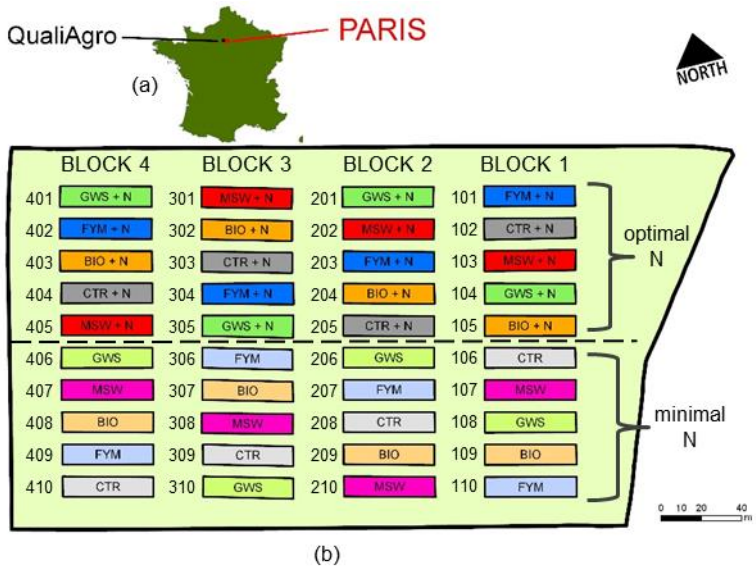

Fig. 1 The 6-ha QualiAgro Field experiment to study the effect of exogenous organic matter applications. (a) Location in the Paris region (France). (b) 40 plots in four repetition blocks, farmyard manure (FYM), municipal solid waste compost (MSW), biowaste compost (BIO) and a co-compost of green waste and sewage sludge (GWS), control (CTR), minimal additional mineral nitrogen (minimal N) and optimal one (optimal N)

The unmanned aerial system

The UAV platform used was a fixed-wing SenseFly® eBee (eBee, SenseFly Parrot group, Cheseaux-sur-Lausanne, Switzerland) (Fig. 2), with a weight of 690 g and a 0.96 m wingspan. The battery life was around 45 minutes enabling coverage of up to 100 ha in one flight at an altitude of 150 m.

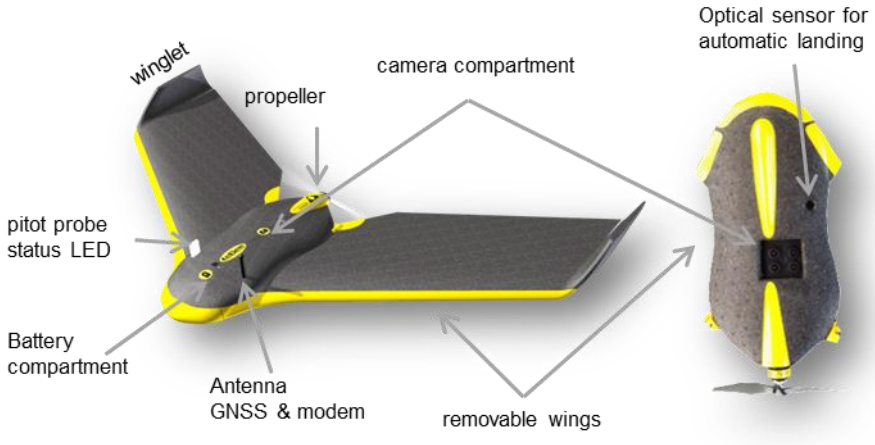

Fig. 2 Sensefly fixed wing eBee UAS platform

The eBee was launched by hand (without catapult) then an autopilot software flew the UAV according to a predetermined flight plan. Position and orientation of the eBee were given by on-board navigation sensors such as an inertial measurement unit (IMU) and a GNNS A high-speed optical sensor on the underside of the UAV was used to detect the proximity of the ground, during automatic linear landing phases. A ground station computer provided UAV flight control by communicating with the eBee using a 2.4 GHz radio modem. The ground station software eMotion 2 ("senseFly - eMotion" n.d.) was used for flight control and also for flight plan preparation. A Canon IXUS 127 HS 16 Megapixels RGB camera (IXUS 127 HS, Canon, Tokyo, Japan) was used for image acquisition. After the flights, eMotion 2 was used to import images and eBee log files to the computer. The UAV flight logs were used for geotagging images with GNSS position, and pitch, roll and yaw orientation.

UAV flights and image acquisition

Two series of flights were done in 2014 on the QualiAgro field with the eBee. The first series was done 6 days after sowing, on April 29, on bare soil at 120 m height above ground from 10h16 to 10h25 UTC. 38 images were shot corresponding to a 40 mm ground resolution and the final mosaic image was 15659 x 11880 pixels. Second series of flights, 126 days after sowing, on August 27, were done in the presence of the maize crop. Two flights were realized at 65 m height above ground, for a total of 414 images having a 20 mm resolution. To allow good 3D reconstructions, overlap rates between successive images were set at 80% forward and 75% side overlap. Twelve ground control points (GCPs) were placed in the field and their positions were measured with a centimetric Trimble Pathfinder Power DGNSS (Pathfinder Power, Trimble, Sunnyvale, USA), averaging each position for one minute . Post-processed differential correction was made with the GPS Pathfinder Office software to improve the accuracy of the GNSS positions, using base data in Rinex format, collected at French RGP reference stations (GNSS permanent network).

Photogrammetric 3D reconstruction

Photogrammetric methods are used to make geometric measurements from aerial images especially to extract the 3D position of objects (Kraus and Waldhäusl 1998). Considering two successive UAV positions 1 and 2 (Fig. 3) separated by a distance b (baseline), where pictures are taken with their optical axes mutually parallel, the observed maize plant P appeared on the first image plane (IP_1) and on the second one (IP_2) respectively at the points P_1 and P_2. These two points projections of the object point P, are called a pair of homologous points. The equipolar plane is defined by the $O_1 P O_2$ triangle and its intersection respectively with IP_1 and IP_2 defines the two equipolar lines EL_1 and EL_2. The disparity d is then defined as the distance between P_1 and P_2 along the equipolar lines. Using triangulation calculation, a direct relation could be found between the depth of the point in the real word (Z_p) and d. It means that 3D structure of rigid objects can be retrieved from their 2D projected positions in pictures as demonstrated by Ullman's Structure from Motion (SfM) theorem (Ullman 1979).

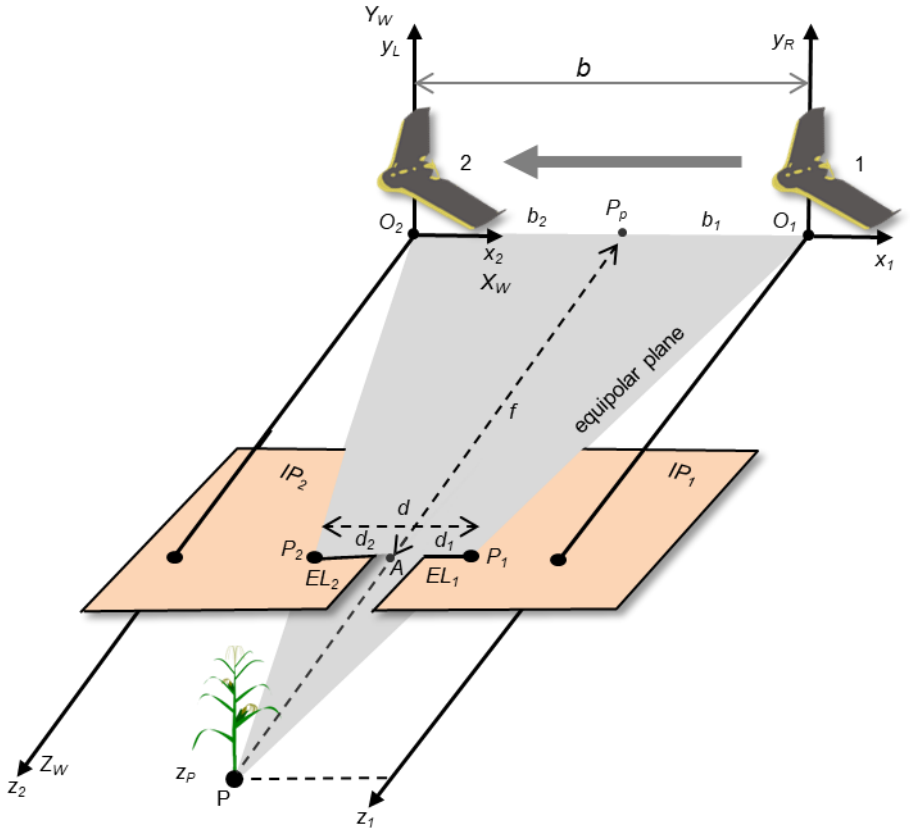

Fig. 3 Photogrammetric triangulation principle for maize plant 3D reconstruction, for two successive UAV positions O_1 and O_2, P the maize plant position, IP_1 and IP_2 the image plane positions, P_1 and P_2 projections of P respectively in IP_1 and IP_2, EL_1 and EL_2 the equipolar lines, d the disparity (distance between P_1 and P_2), b the baseline (distance between O_1 and O_2)

The automatic 3D reconstruction procedure began by the detection of key points in the images and the construction of their feature descriptor. Next, a feature matching step found corresponding pairs between images, allowing definition of the camera pose and 3D scene structure. In order to be matched, the descriptors need to be invariant between pictures. The scale invariant feature transform (SIFT) is one of the most commonly used descriptors (Lowe 2004). The resulting output is a 3D points cloud. An extra step is generally carried out to densify this point cloud (Fig. 4).

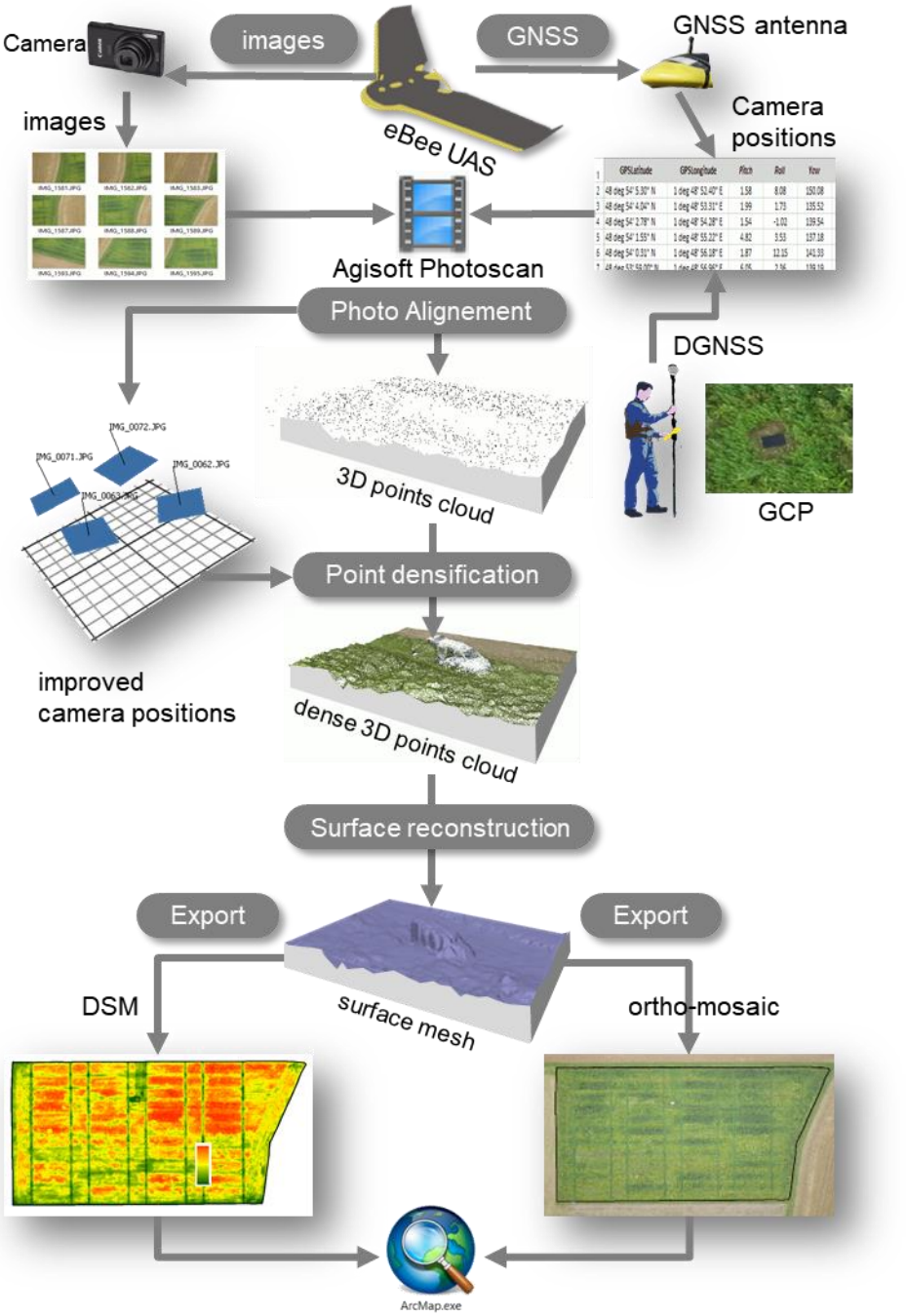

Fig. 4 General processing workflow from UAV images to ortho-mosaic and digital surface model (DSM). Photogrammetric processing uses, as input, the images as well as the camera positions given by the global navigation satellite system (GNNS) antenna. Ground control points (GCP) were placed in the plot, to be visible in the images. Their precise position was measured with a differential GNSS (DGNSS) to improve the georeferencing of the data.

An orthophoto was exported based on the 3D model and the original pictures as well as a DSM that represented the scene surface in a raster format. In this study, the Agisoft Photoscan Professional 1.2.6 software ("Agisoft Metashape" n.d.) was used for the photogrammetric processing. To improve data georeferencing, 12 ground control points (GCPs) had been distributed evenly within the field, before each UAV flight. The precise position

of each GCP's center was obtained using a rod-mounted centimetric Trimble Pathfinder Power DGNSS. The rod had a spirit level to guarantee a few centimeters accuracy. Photoscan parameters were fixed to: (i) 12 markers used to optimize camera positions and orientation data, which allowed better model reconstruction and precise georeferencing; (ii) highest accuracy for the "Align Photos" step and (iii) ultra-high quality for the "Build Dense Cloud" step with the mild depth filtering mode to preserve small details in the 3D cloud. A Dell precision T7910 workstation was used, with an Intel dual Xeon 2.4 Ghz processor with 20 cores, 128 GB RAM and an NVIDIA Quadro M6000 24 GB graphic card.

Photogrammetric crop height estimation

The DSM produced from the flight of April 29 represented the bare soil surface (Z_s) (Fig. 5a) and the one of August 27 represented the maize surface (Z_m) (Fig. 5b). The height of maize plants (Fig. 5c) can then be deduced from the difference between Z_m and Z_s. The bare soil DSM was smoothed within a 1 m neighborhood to limit the non-permanent effects of soil labor marks on the topography. Making a flight on bare soil four months before the flight on crop is an important operational constraint. To test if the bare soil DSM can be replaced, DEMs produced by the French national institute of geographic and forest information (IGN) were tested: the IGN BD ALTI® DEM (25 m resolution) (BD ALTI, IGN, Saint-Mandé, France), IGN RGE ALTI® DEM (5 m resolution) (RGE ALTI, IGN, Saint-Mandé, France), and the RGE ALTI interpolated to a one-meter resolution using the ArcGIS 10.1 (ArcGIS 10.1, Esri, Redlands, USA) resample function with bilinear interpolation. Four maize height models (*MH)* were calculated based on the data used as a topographic reference: (i) MH_{uav} using the DSM produced by the UAV, (ii) MH_{ign25} using the 25 m resolution IGN DEM, (iii) MH_{ign5} using the 5 m resolution IGN DEM and (iv) MH_{ign1} using the 1 m resolution IGN DEM.

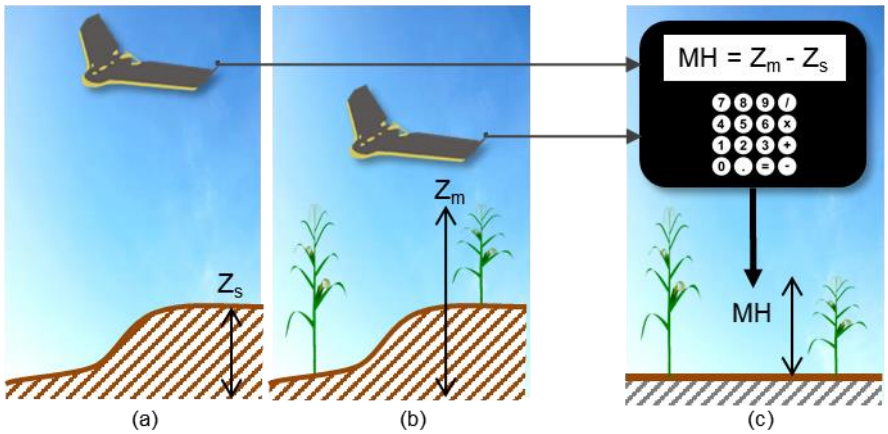

Fig. 5 Photogrammetric maize height estimation method. UAV flight of April 29 to calculate bare soil surface (Z_s) (a) and the one of August 27 to calculate the maize surface (Z_m) (b). Maize height (MH) (c) was the difference between Z_m and Z_s

Field data collection

To validate the photogrammetric estimate of the *MH*, 38 reference measurements (MH_{ref}) were done in the Qualiagro field (Fig. 6), with a 2.5 m wooden rule, including a spirit level. The plant height was measured from

the ground to the base of the flower at the apex of the stem end. The precise position of each measurement was obtained using the Trimble Pathfinder Power DGNSS.

(a) (b)

Fig. 6 Maize height reference measurements in the field using a rule with a spirit level (a), each measurement was precisely located with a centimetric DGNSS (b)

Manual harvest in 40 plots was conducted on October 22 and 27 for yield estimation. Each plot contained 12 rows 0.8 m spacing, of which the six central rows were sampled to prevent side effects (Fig. 7). The ears and stalks were counted and collected in five sub-plots; each sub-plot consisted of two maize rows over a length of 2.5 m, which represented a total of 25 m of maize on each of the 40 plots. The geolocation of each sub-plot was measured with the Trimble DGNSS. All aerial parts taken from sampled sub-plots were weighed. For each plot, a sample of stalks, stems, leaves and grains was also taken to be analyzed. Weighing of grains, stems and leaves were made fresh and after drying at 50°C.

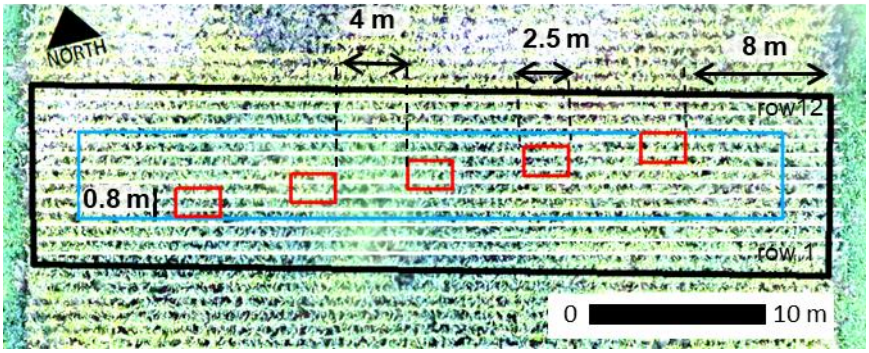

Fig. 7 Map of the five sampling areas in one of the 40 QualiAgro plots (Fig. 1). The black rectangle is the boundary of the plot (45 x 10 m), the white lines represent the 12 maize rows present in the plot. To avoid edge effects, analysis was conducted on the six central rows only (lines 4 to 9, blue rectangle). Red rectangles depict destructive sampling areas.

Maize height analysis

CSMs and MH_{ref} layer were analyzed in ArcGIS 10.1. To consider a possible small inaccuracy of the DGNSS location, the *CSMs* were filtered with the maximum value in a circular neighborhood of 0.3 m radius around each pixel. MH_{ref} measurements were made along the stem which corresponded to the highest point of the leaves. The "Zonal Statistics as Table" function, of the ArcGIS 10.1 Spatial Analyst extension, was used to extract *MH* from the filtered CSM pixel closest to each MH_{ref} position. The dataset was divided into two equally sized subsets: (i) one for height calibration calculating a linear regression between *MH* and MH_{ref} values, and (ii) one for validation between calibrated height MH_{cal} with the previous linear model and MH_{ref} values. Linear regression equations were built and the coefficient of determination (R^2) was calculated. For validation dataset, the root mean square error of prediction (RMSEP) (Eq. 1) and the relative root mean square error of prediction (RRMSEP) (Eq. 2) were calculated.

$$RMSEP = \sqrt{\frac{\sum_{i=1}^{n}\left(MH_{i,ref} - MH_{i,cal}\right)^2}{n}} \quad (1)$$

$$RRMSEP = \frac{RMSEP * 100}{\overline{MH_{i,ref}}} \quad (2)$$

Where $MH_{i,cal}$ is the calibrated maize height obtained by applying the regression equation to the CSM at the i^{th} position., $MH_{i,ref}$ is the reference maize height measured in the field at the same i^{th} position, *n* is the number of height measurements and $\overline{MH_{i,ref}}$ is the average reference height.

Yield data analysis

To compare the CSMs with the yield measurements acquired during the harvest, the 480 maize rows (12 rows x 40 plots) were first manually digitized in ArcGIS, using the 20 mm resolution UAV orthophoto. For each maize row, a 0.3 m wide buffer polygon was created, with the ArcGIS buffer tool. The buffer zones were then intersected with the sampling sub-plots to match the maize harvesting areas (Fig. 8). The raster $MH_{uav,\ cal}$ values

were summarized within the previous areas using the ArcGIS “Zonal Statistics as Table” function. The results were compared to yield harvest data on the 40 plots.

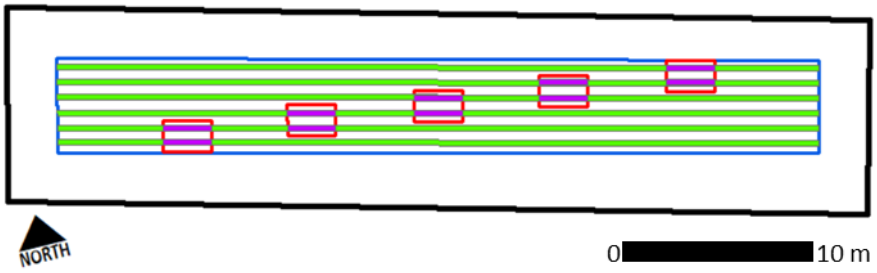

Fig. 8 Buffer zones for yield analysis around maize rows (green) are limited to sub-sampling plots (red), resulting in limited buffer areas (pink)

Correlations between maize heights and green biomass or grain yield, both fresh and dry, were analyzed. As QualiAgro field is organized in to four repetition blocks, the first two (20 plots) were used as the calibration dataset and the remaining ones as the validation dataset. Three regression models were tested: exponential, power and generalized additive model (GAM). GAM well adapts the fitted curve to the data in the case where a parametric equation does not fit sufficiently. Exponential and power models were calculated with Microsoft Excel while GAM was calculated with R 3.3.1 (R Development Core Team 2016) using the mgcv package (Wood 2017). In the case of GAM, unlike the exponential and power models, the result of the modelling is not an equation. The "predict ()" function was used to build a look up table (LUT) of the predicted yield values. This LUT was used for model validation in Excel and for creating yield maps from the GAM model in ArcGIS. The "INDIRECT ()" function in Excel was used to extract the yield value from the LUT corresponding to a maize height rounded to centimeters. In ArcGIS, the spatial analyst “Reclass by Table” function was used to convert the MH raster to a new yield grid using the LUT. Scatter plots were built showing the regression equation, the coefficient of determination (R^2). The RMSEP and RRMSEP were calculated for the validation dataset for all the cases. The different models were compared considering their performance (RRMSEP).

Spatial analysis of the yield map

To compare spatial variability, yield maps were derived from destructive sampling and the UAV data, based on dry grain yield per plot, divided into five classes. Three yield maps were derived: one from destructive sampling in the sub-plots, one from UAV yield estimation based on the GAM model considering the sub-plots, and one from the UAV yield estimation considering the entire rows in each maize plot (Figure 8). The comparison of these maps was used to analyze the impact of the yield measurements sampling on the QualiAgro experiment predictions, plot by plot. Finally, a 9-class map was created from the UAV-estimated yield map at the pixel scale. Two zonal histograms per plot were compared, one calculated in the five sub-sample plots and the other over the entire plot. These results were analysed for two contrasting plots.

Results and discussion

After post processing against a reference station, GCP horizontal accuracy was 0.029 m. As the antenna height was 3 m, a two degrees maximum error with respect to the vertical caused a ground error of 0.105 m. It is reasonable to assume that the total horizontal error was around 0.15 m.

Photogrammetric reconstruction

The 3D sparse cloud construction of the maize plot with the highest accuracy, took 8 h and 11 min of processing time from 414 images (Table 1) in Agisoft Photoscan. The result cloud contained more than 4 million points. The densification step in ultra-high quality took 8 h and 35 min and the final dense cloud contained 676 million points.

Table 1 Parameters report for Photoscan reconstruction with the 414 UAV images taken on August 27th, for DSM creation in the presence of maize

General	Cameras	Aligned cameras	Markers	Coordinate system	Rotation angles
	414	414	12	WGS 84	Yaw, Pitch, Roll
Point cloud	Points	Accuracy	Matching time	Alignment time	RMS reprojection error
	4,410,369	Highest	7 h 49 min	22 min 47 sec	0.169
Dense Point Cloud	Points	Quality	Depth filtering	Depth maps time	Dense cloud time
	676,282,349	Ultra High	Mild	3 h 31 min	5 h 04 min

The final DSM and image mosaic were 29740 x 24220 pixels size with a ground resolution of 20 mm per pixel. The mean XY positioning error in the final mosaic estimated by Photoscan was 0.098 m. Figure 9 shows the two final mosaics, the one on bare soil (April 29) and the one on crop (August 27).

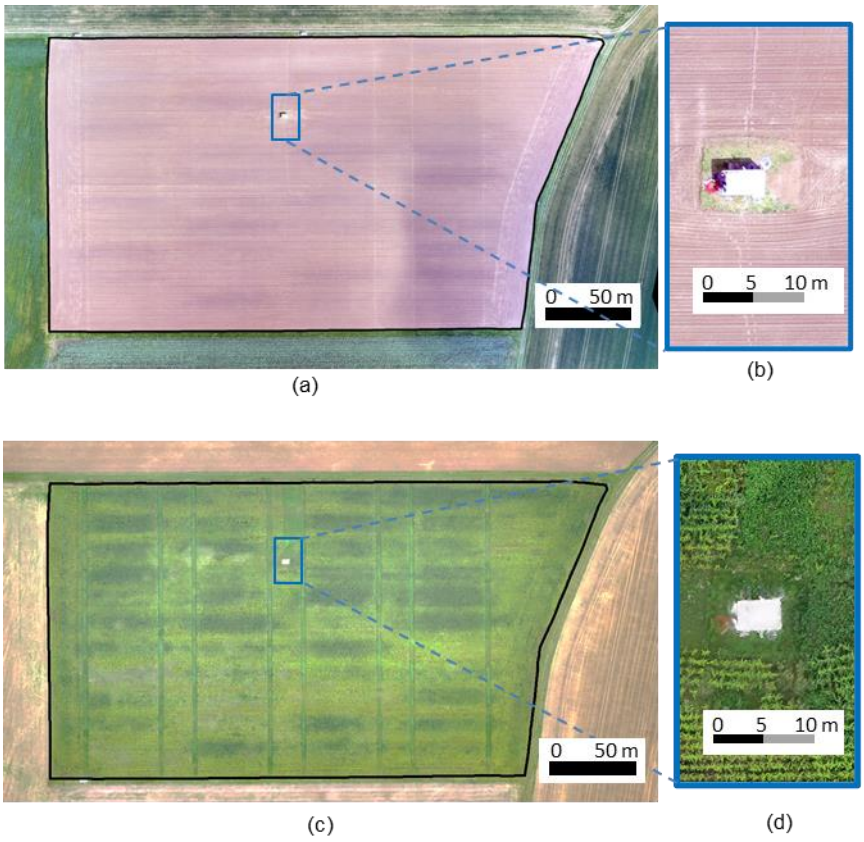

Fig. 9 Final 15659 x 11880 pixels mosaic on bare soil (April 29) with a 40 mm ground resolution (a), final 29740 x 24220 pixels mosaic on maize (August 27) with a 20 mm ground resolution (c); (b) and (d) show a zoom on an 28 x 16 m area centered on the building containing the measuring sensors of the plot

Maize Height estimations

The four *MH* models were calculated according to the topographic data used: MH_{uav}, MH_{ign25}, MH_{ign5} and MH_{ign1}. Figure 10 presents the MH_{uav} map example using the UAV topographic map.

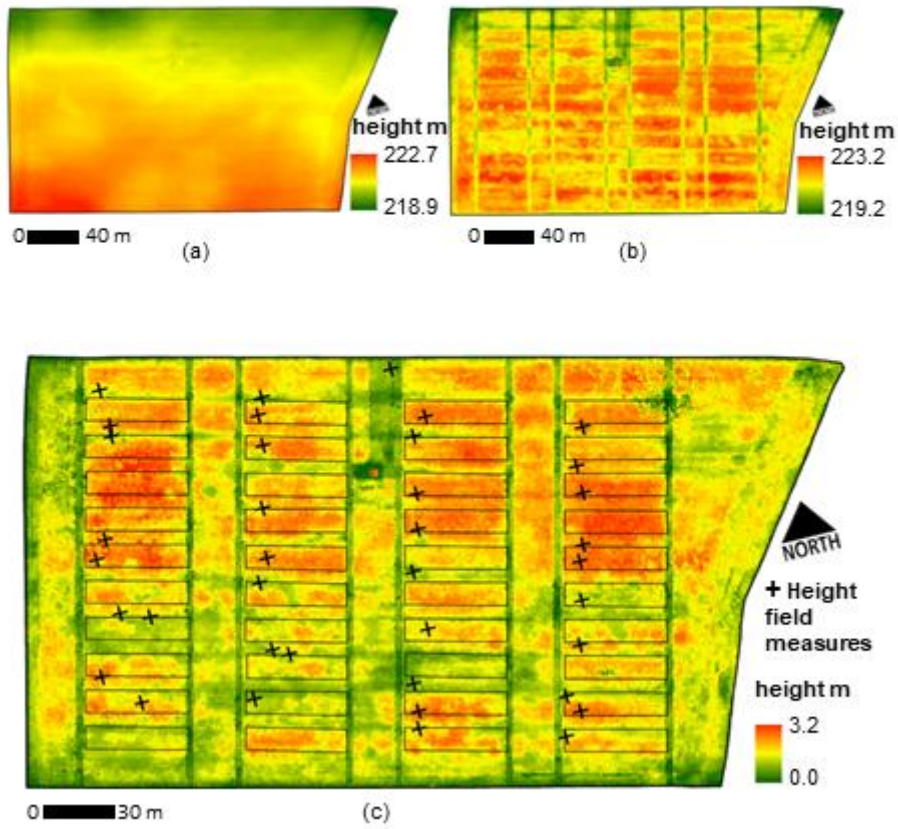

Fig. 10 Maize Height (MH_{uav}) creation (c) from the difference between Z_m (b) and Z_s (a)

Figure 11 presents the four calibration equations obtained by linear regression between the *MH* models and the in-field reference maize height measurements. Coefficients of determination (R^2) were all between 0.89 and 0.9. There was a strong correlation between the maize height models calculated from the UAV data and the in-field measurements. In the regression equations, there was a bias between 0.43 and 0.65 m. This bias can easily be explained because the height measurements in the field were made from the ground to the base of the top flower, while in top view UAV images (20 mm resolution), the flower has little surface and the leaves located a few tens of centimeters lower were detected as the top surface. Bendig et al. (2014) also noted this difficulty to compare the reference height measure in the field with the height extracted from the CSM in a study on barley. They averaged field and CSM height values over an area of a few square meters to compare them, but field measurements were made only on the highest part of the plant whereas CSM heights integrate all parts of the crop. In this study, unlike Bendig et al. (2014), field height measurements for CSM calibration were plant-level point measurements. Comparing the height measurement with the correct CSM pixel required a georeferencing with an accuracy of a few centimeters. Adding the GNSS error in the field (0.15 m) to the error related to the construction of the image mosaic (0.098 m) gives a total error of 0.25 m. To limit the effect of this error, CMSs were filtered with the maximum value in a circular neighborhood of 0.30 m radius around each pixel before calibration regression.

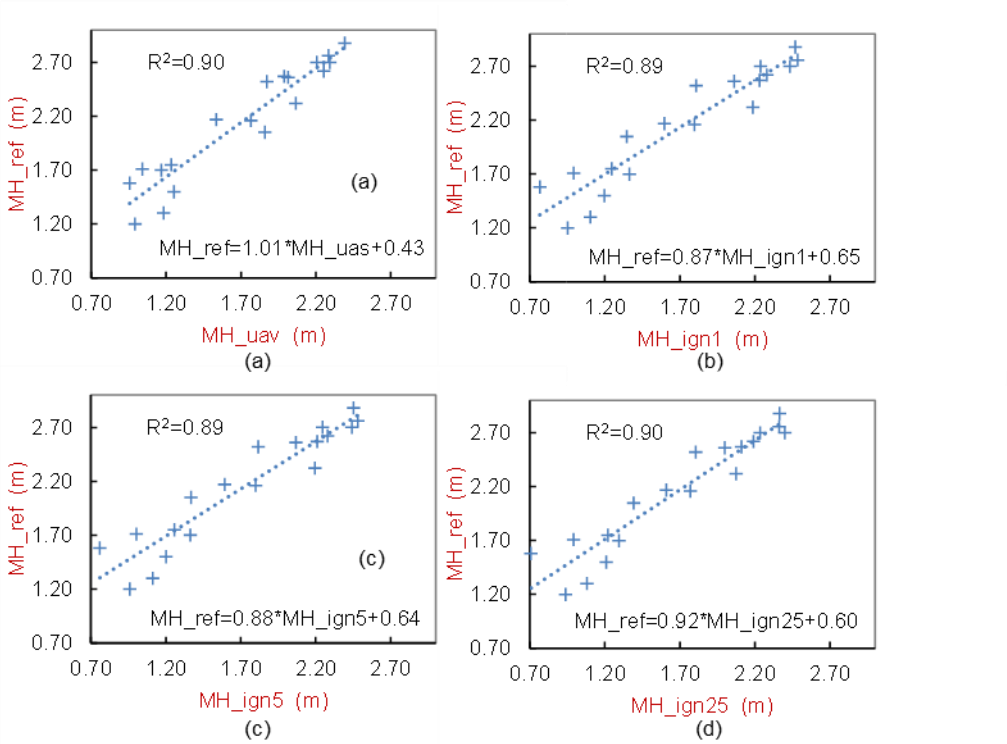

Fig. 11 Regressions between in field maize height reference measurements and the four MH models: MH_{uav} *(a)*, MH_{ign1} *(b)*, MH_{ign5} *(c)* and MH_{ign25} *(d)*

Model validations are presented in Figure 12. The maize height prediction error (RMSEP) was 0.16 m (RRMSEP=7.2 %) for the MH_{uav} model. This result is consistent with those found in the literature. Li et al. (2016) had similar results using 20 mm resolution UAV images on a maize crop. They also found good correlation between UAV derived crop height and field measurements (R^2 = 0.88), using a stepwise linear regression model. They found an RMSE of 0.16 m (RRMSE=6.40 %). Chang et al. (2017) studied crop height of Sorghum with a similar approach. Their result showed an RMSE of 0.33 m. Yue et al. (2017) found a satisfactory regression (R^2=0.69) between CSM and measured height for winter wheat canopies. Holman et al. (2016) compared UAV modelled CSM to crop heights measured from a terrestrial laser scanner (TLS) and from a 2 m rule. Their study was conducted on a winter wheat field phenotyping experiment. They obtained good results with crop height RMSE ranging from 0.02 to 0.1 m. It is not easy to directly compare the height estimation performance of these studies, because they were done on various crops of different size, possibly at different phenotypical stages.

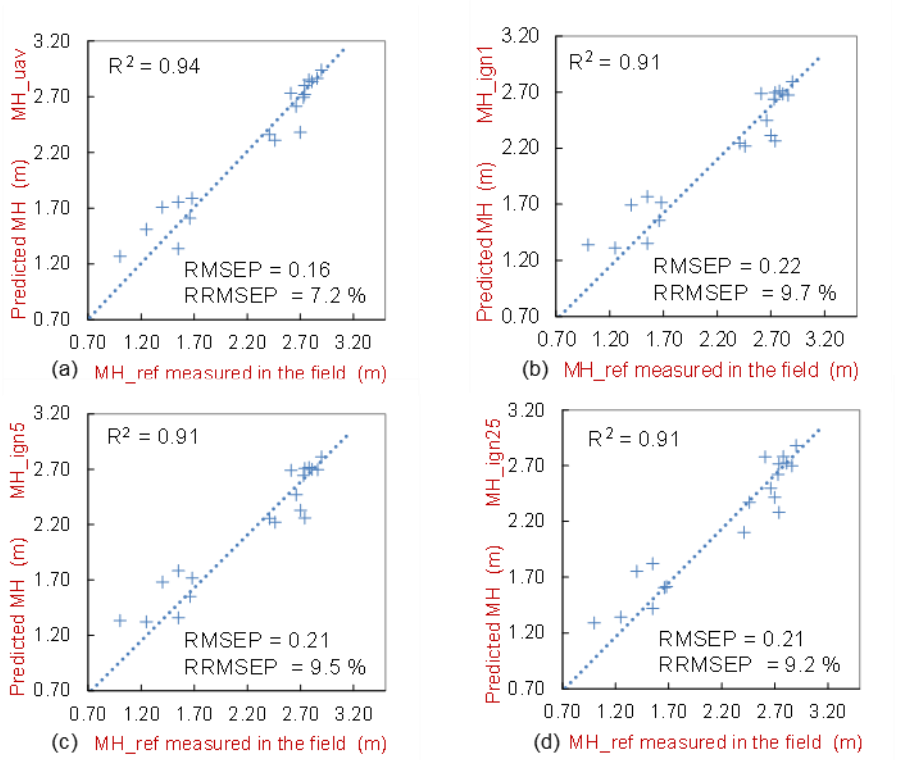

Fig. 12 Validation of the relationships (Fig. 11) for MH models: MH_{uav} *(a)*, MH_{ign1} *(b)*, MH_{ign5} *(c)* and MH_{ign25} *(d)*

Height RMSEP obtained with the three *IGN* models (MH_{ign25}, MH_{ign5} and MH_{ign1}) ranged from 0.21 to 0.22 m to compare with the 0.16 m RMSEP obtained with MH_{uav} model. The UAV DSM gave the most accurate height estimate but it was only slightly better than with IGN models. Using DSM topographic data instead of a UAV flight on bare soil, can therefore be considered as satisfactory, which simplifies the method. Nearly identical performance was obtained regardless of the DEM resolution (from 1 to 25 m). For this, the local topographic slope must be small at the scale of the DSM cell, for the error induced on the maize height estimate to be negligible. This was the case for the QualiAgro experiment, which was a relatively flat field. For example, for a one-meter resolution DSM, to have a maximum error in height of 0.05 m, the local slope must be less than 5%.

Grain and biomass yield prediction

Figure 13 presents the scatter plots of the regression models: exponential (a), power (b) and GAM (c) for dry grain yield prediction. The performance of all the prediction models for grain and green biomass yields, dry and fresh, is presented in Table 2. Whether for grain or biomass yield, fresh or dry, the models are always ranked in the same order according to their performance (RRMSEP): the GAM model is the most efficient, followed by the power model and finally the exponential one. The results showed that the biomass measurements have a strong correlation with the MH estimated by UAV, with R^2 ranging from 0.83 to 0.92 for the different models and RRMSEP calculated with a validation data subset range from 13.03 to 20.23 %. The best model was

obtained for dried biomass prediction using GAM, with a RMSEP of 0.6.1 t ha^{-1} (RRMSEP = 13.03 %) and an

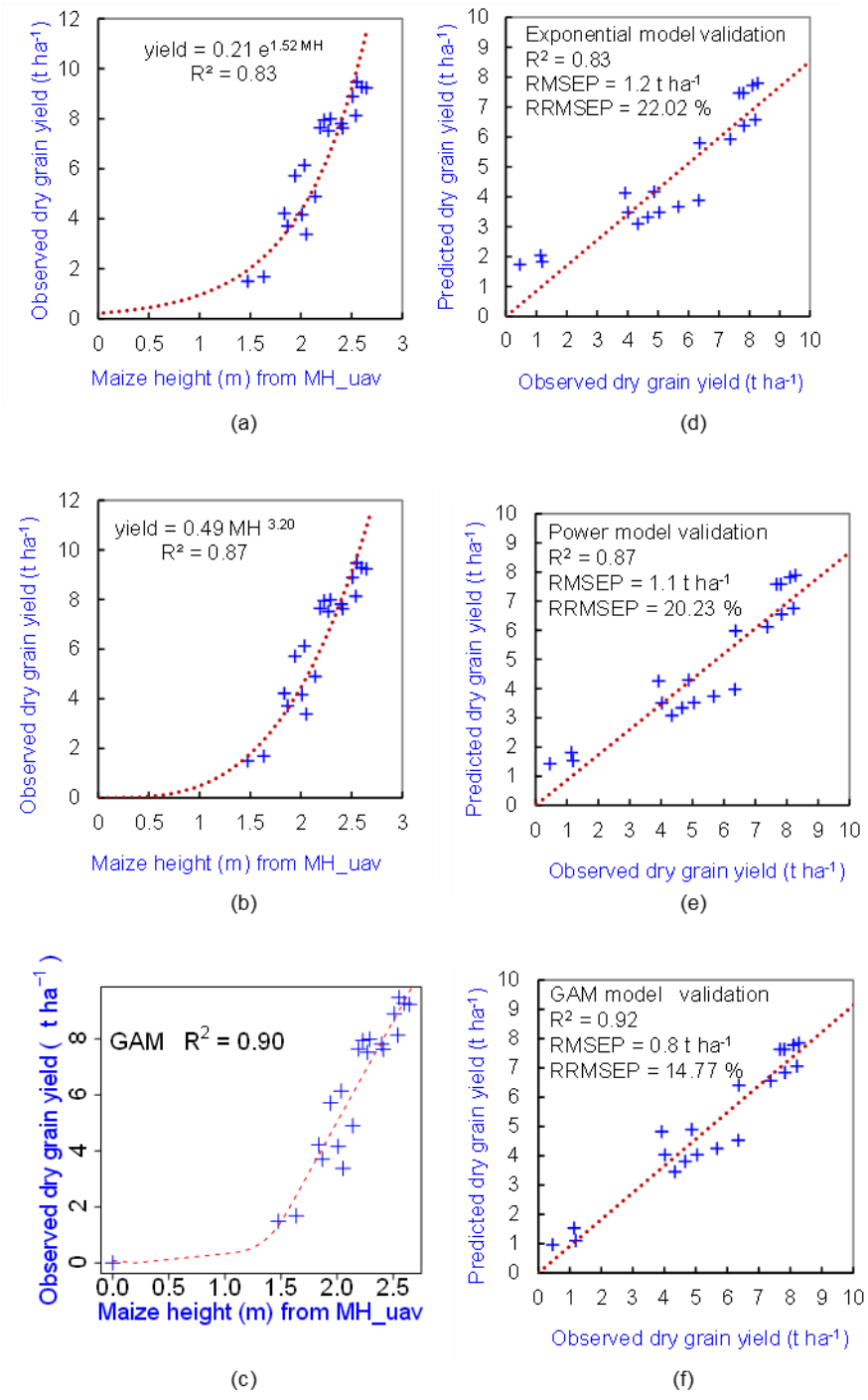

R^2 of 0.9.

Fig. 13 Prediction models for dry grain yield. Calibration of the models: exponential (a), power (b) and GAM (c) on the first 20 plots. Validation of models: exponential (d), power (e) and GAM (f)

Li et al. (2016) had similar results with a random forest regression model between MH and dried (85°C) maize biomass, with an R^2 of 0.78 and an RMSE of 2.7 t ha^{-1} (RRMSE = 16.66 %). Their result may be a little over-estimated as they did not validate it on an external independent dataset. Bendig et al. (2014) achieved a RRMSEP of 54.04 % and an R^2 of 0.71 for biomass prediction using an exponential regression, in a summer

barley experiment. The quality of yield predictions is undoubtedly dependent on the type of crop and the period of measurement.

Table 2 Performance of grain and green biomass yield prediction models

Grain (G) Biomass (B)	Dry (D) Fresh (F)	Model	R^2 Model	RMSEP validation t ha^{-1}	RRMSEP validation %	RRMSEP difference D - F	RRMSEP difference B – G
G	D	exponential	0.83	1.20	22.02 %	+ 0.21 %	- 4.54 %
G	D	power	0.87	1.10	20.23 %	+ 0.10 %	- 4.83 %
G	D	GAM	0.90	0.80	14.77 %	+ 0.06 %	- 1.74 %
G	F	exponential	0.83	1.79	21.81 %	x	- 1.62 %
G	F	power	0.87	1.66	20.13 %	x	- 1.8 %
G	F	GAM	0.90	1.21	14.71 %	x	+ 0.36 %
B	D	exponential	0.86	0.82	17.51 %	- 2.68 %	x
B	D	power	0.90	0.72	15.40 %	- 2.93 %	x
B	D	GAM	0.90	0.61	13.03 %	- 2.04 %	x
B	F	exponential	0.88	4.07	20.19 %	x	x
B	F	power	0.91	3.70	18.33 %	x	x
B	F	GAM	0,92	3.04	15.07 %	x	x

There was little difference in performance (RRMSEP) between models built with fresh biomass or grain with models built after drying. This difference was less than 0.21 % for grain models and less than 2.93 % for biomass models. This negligible difference could be explained by a few humidity variations that have been measured. Throughout the QualiAgro experiment, the average grain moisture was 33.99 % with a coefficient of variation of 3.95 % and the average biomass moisture was 75.78 % with a coefficient of variation of 2.59 %. In contrast, Bendig et al. (2014) found better results with fresh biomass rather than with dried biomass for barley. The prediction is still slightly better for the biomass models (lower RRMSEP) compared to the grain models, except for the fresh GAM model where the difference is nearly zero (+ 0.36%). This difference ranges from - 1.62 to - 4.83 %.

Spatial analysis of the yield maps

Figure 14 presents maps of mean grain yield in the 40 QualiAgro plots in five classes. The first map (Fig. 14a) was calculated from the MH UAV measurements (GAM) and the second one (Fig. 14b) from the field measurements. Each of the 40 plots is in the same category for both maps. In the case of the third map (Fig. 14c), the yield estimate was based on the maize height measured by the UAV along the entire rows, in contrast to the other two maps that were based on measurements in the five sampling sub-plots. Six plots of this third map were in a different category compared to the other two maps, because the sampling areas were not the same for this map.

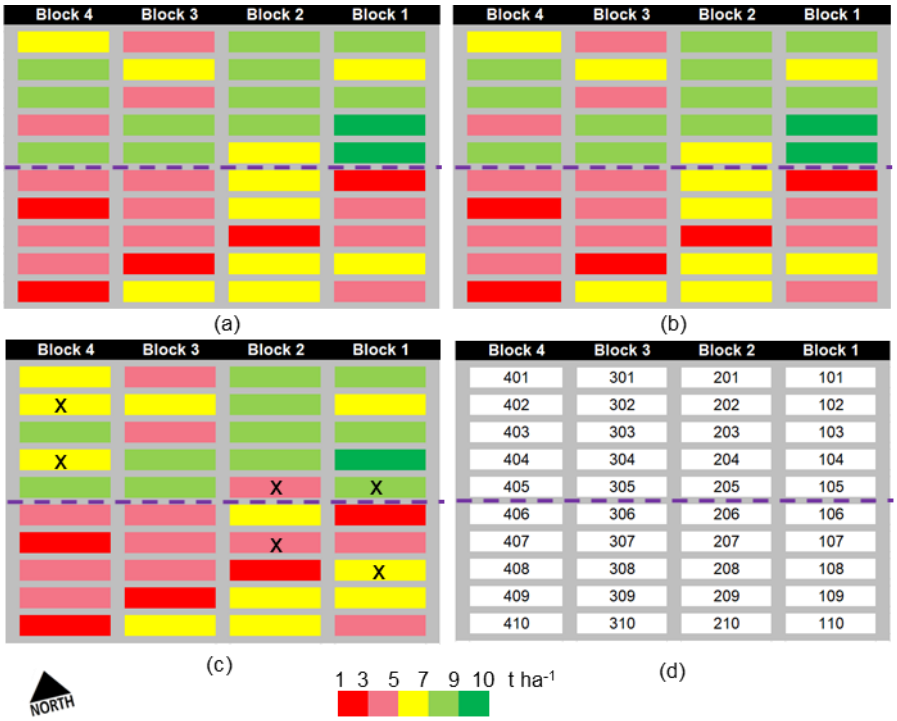

Fig. 14 Grain yield maps in five classes (mean value per plot) from MH estimated by UAV (GAM model) in (a) and from field measurements in (b), estimates based on the five sample sub-plots for (a) and (b), while (c) was the same as (a) but using MH and the complete maize rows in each plot. Crosses indicate estimates that are different from field measurements (b), (d) numbering of the 40 plots distributed in the four blocks

Figure 15 shows the 40 QualiAgro plot maps made with the GAM model for predicting grain yield (dried) and Table 3 presents the mean yields and coefficients of variation calculated from these maps in each plot. The average predicted yield over the entire QualiAgro plots was 5.6 t ha^{-1} while the same average yield measured from 200 samples in the field was very close with a value of 5.5 t ha^{-1}. The mean yield per plot ranged from 1.4 (plot 407 MSW) to 9.2 t ha^{-1} (plot 104 GWS+N).

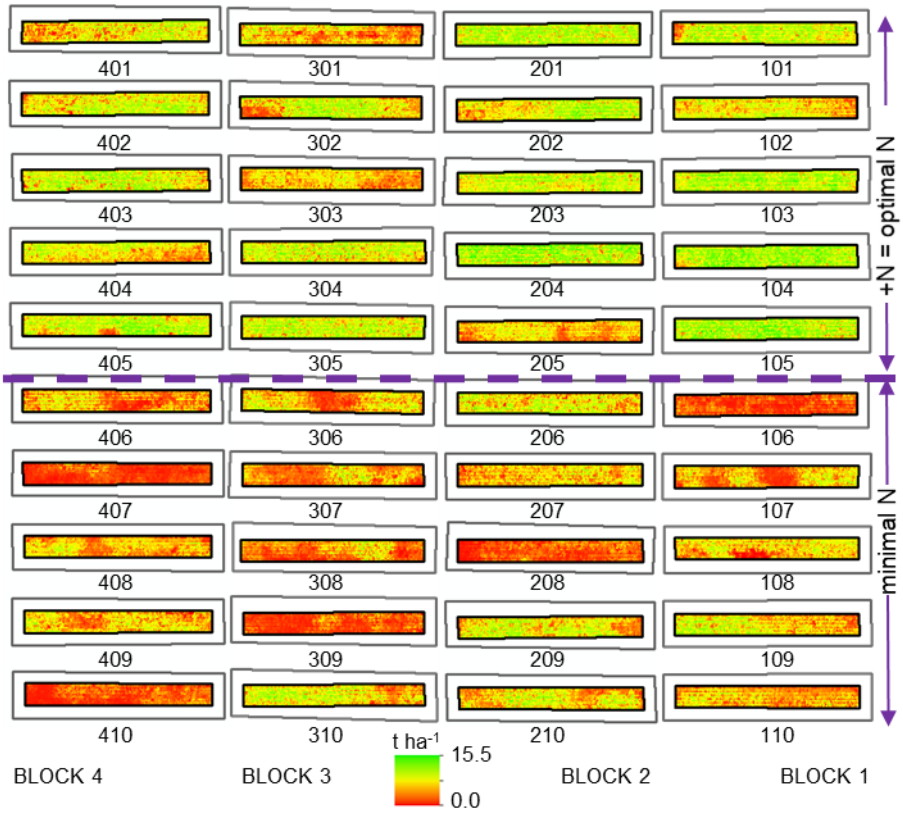

Fig. 15 Dried grain yield prediction maps in the 40 QualiAgro plots calculated using the GAM model

Table 3 Basic statistics of grain yield prediction with GAM model per QualiAgro plot (average yield in t ha^{-1} and coefficient of variation in percentage) for the different treatments shown in Figure 1

Plot	Avg	CV	Plot	Avg	CV	Plot	Avg	CV	Plot	Avg	CV
401 GWS+N	6.13	40.8	301 MSW+N	4.58	52.4	201 GWS+N	8.41	22.0	101 FYM+N	7.66	28.9
402 FYM+N	6.96	32.0	302 BIO+N	6.70	42.9	202 MSW+N	7.18	33.1	102 CTR+N	5.87	37.0
403 BIO+N	7.4	32.3	303 CTR+N	4.76	40.7	203 FYM+N	7.63	25.4	103 MSW+N	8.54	22.6
404 CTR+N	5.93	37.0	304 FYM+N	7.27	30.5	204 BIO+N	8.94	25.9	104 GWS+N	9.24	20.7
405 MSW+N	7.76	30.4	305 GWS+N	7.58	28.0	205 CTR+N	4.90	40.6	105 BIO+N	8.90	23.9
406 GWS	3.69	61.2	306 FYM	4.39	57.3	206 GWS	6.48	37.7	106 CTR	1.72	67.1
407 MSW	1.38	72.9	307 BIO	3.67	58.8	207 FYM	4.88	43.5	107 MSW	4.16	60.3
408 BIO	4.37	47.3	308 MSW	3.25	66.0	208 CTR	2.01	69.4	108 GWS	5.27	46.2
409 FYM	4.95	46.5	309 CTR	1.81	73.6	209 BIO	6.37	40.2	109 BIO	5.92	42.6
410 CTR	1.89	70.7	310 GWS	6.19	41.3	210 MSW	5.34	46.3	110 FYM	4.14	49.0

The average yield over all the plots that received a minimal additional mineral N dose was 4.1 t ha^{-1} while it was 7.1 t ha^{-1} for the plots that received an optimal one. Fig. 14c and Fig. 15 show the green dominant color in the northern part (optimal N) of the field, corresponding to higher yield, and red dominating the southern part (minimum N) with lower yield. The calculated plot-per-plot coefficients of variation range from 20.7 to 73.6% with an average value of 43.6% reflecting the intra plot variability of the yield.

Figure 16 presents an estimated grain yield map in 9 classes for two plots. For each map, two zonal histograms were calculated: one for the whole plot maize rows (black rectangle) and one for the five sampling sub-plots (blue rectangles). In the case where the five sub-plots are representative of the variability of all the plot rows, the two histograms should be identical. For parcel 405, it is nearly the case, there is little difference between the two histograms (maximum 23% for class 2); for parcel 208 there are pronounced differences particularly for the classes one in red (82%) and two in dark orange (50%). The average yields on the entire plot and in the five sub-plots were: (i) 7.75 and 7.76 t ha^{-1} for parcel 405 (0.13 % error) and (ii) 2.01 and 2.51 t ha^{-1} for parcel 208 (24.86 % error). Several large red and dark orange areas in parcel 208 explain this error, mainly located in the west and south of the parcel, outside the five sampling plots. Classes one and two are thus under-represented in the sampling plots. Similarly, classes 8 and 9 are over-represented in sampling plots compared to the whole plot. Intra-field spatial variability of yield can be relatively large, especially in the case of a field experiment, where different experimental farming practices can lead to contrasting effects. These variabilities can be localized in the plot, as for example in the case of attack by destructive pests, crop disease, presence of weeds or errors during agricultural practices such as defect of sowing or sub-dose (over-dose) of product. This was particularly the case in 2014 on QualiAgro with the presence of many weeds due to the transition to organic farming practices that year. The method will be applied again on QualiAgro with a better control of weeds. It is therefore very difficult to design a crop monitoring sampling that can take into account these possible spatial variabilities, which are almost random. For this case, high spatial resolution UAV imagery is particularly useful.

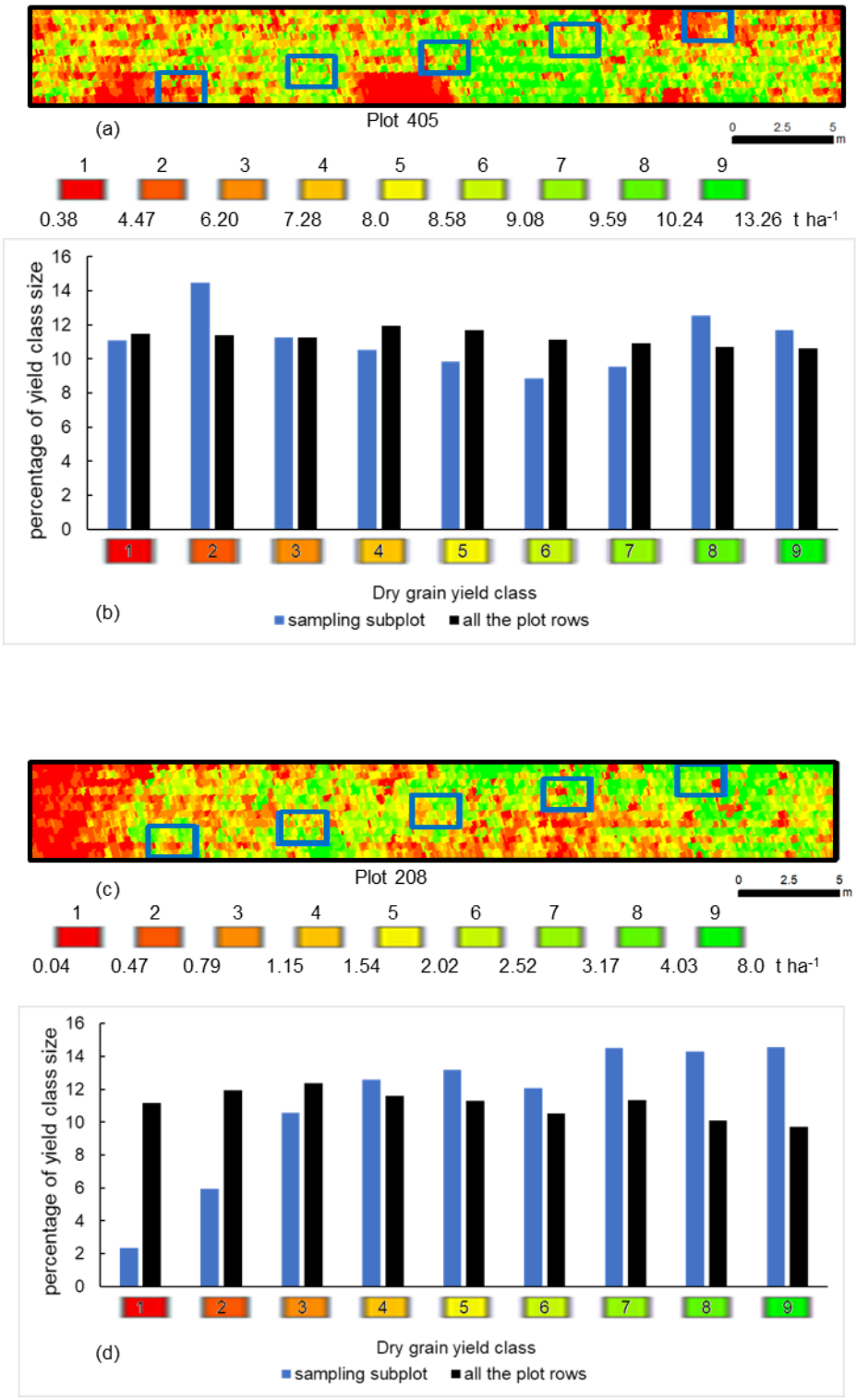

Fig. 16 Estimated grain yield map in 9 classes for plot 405 (a) and for plot 208 (c). For each map, two zonal histograms were calculated: one for the whole plot maize rows (black rectangle) and one for the five sampling sub-plots (blue rectangles). Histograms for plot 405 (b), histograms for plot 208 (d)

Conclusions

This work shows the potential of using crop height estimation from UAV images to spatially predict maize yield for better variability analysis in a field experiment. The method that was used to estimate crop height was based on two UAV flights on an agricultural plot, one in the presence of maize and the other on bare soil. A 3D photogrammetric approach was chosen for deriving DSMs from the UAV imagery. Crop height was obtained by difference of the two DSMs. The obtained maize prediction error was 0.16 m (RRMSEP=7.2 %) based on 38 ground reference measurements, demonstrating accurate crop height prediction. DEMs produced by the French Institute of Geography were also used instead of bare soil flight data. Maize height prediction error obtained was 0.21 m (RRMSEP=9.2 %). Since little precision is lost (~0.1 m) when using basic topographic data, it is a valid alternative as it reduces the number of necessary UAV flights. Based on crop height, exponential, power and GAM regression models were used to predict above-ground biomass and grain yield (fresh or dry). The best result was obtained with the GAM model with an error of 0.8 t ha^{-1} (RRMSEP=14.77 %) for dried grain yield prediction, based on 100 sub-plot ground validation measurements. Mean yield value per plot was estimated from UAV data in sub-plots, which were also manually harvested, and using all rows within one plot. Considering the yield estimate on all the plot rows as the closest to reality, the manual method is less accurate with differences of up to 25% on one plot. This case mainly occurs where a local heterogeneity is poorly represented in the sub-plots. Overall, 6 out of 40 plots showed a differing yield, when classifying manual and UAV-derived yield into five classes. Therefore, the UAV estimate improved overall results by 15%, leading to a better comparison of the 10 agronomic treatments of the QualiAgro experiment.

Monitoring of agronomic experiment such as QualiAgro could be improved by integrating yield estimates using UAV with several advantages: (i) automation of biomass measurements; (ii) a better spatial representativeness of the measurements per plot, (iii) a detailed sub-plot cartography, (iv) reducing the number of harvesting sub-plots (used to calibrate the UAV maps); and (v) allow non-destructive monitoring throughout the cropping season.

Acknowledgments The authors are grateful to Jean-Noel Rampon and Vincent Mercier, in charge in 2014 of the daily management of the field experiment, for the maize sampling and analysis.

Funding This publication benefited from financial support from the scientific direction of AgroParisTech and from the French national observatory networks “SOERE PRO” part of the AnaEE-France project of the French Investments for the Future (Investissements d'Avenir) program, implemented by the French National Research Agency (ANR) (ANR-11-INBS-0001). The field experiment QualiAgro has been managed since 1998 within a cooperation between INRAE and Veolia Research and Innovation.

Author’s contributions SH and JMG designed the experiments. Experiments were performed by JMG, JM and DH. JMG drafted the manuscript with help and contributions from all other authors. Analyses, figures and tables were mainly performed and produced by JMG. All authors read and approved the final manuscript.

Compliance with ethical standards

Conflict of interest The authors declare that they have no conflict of interest.

References

Agisoft Metashape. (n.d.). https://www.agisoft.com/. Accessed 16 June 2020

Barnes, E. M., Sudduth, K. A., Hummel, J. W., Lesch, S. M., Corwin, D. L., Yang, C., et al. (2003). Remote- and Ground-Based Sensor Techniques to Map Soil Properties. *Photogrammetric Engineering & Remote Sensing*, *69*(6), 619–630. doi:10.14358/PERS.69.6.619

Bendig, J., Bolten, A., Bennertz, S., Broscheit, J., Eichfuss, S., & Bareth, G. (2014). Estimating Biomass of Barley Using Crop Surface Models (CSMs) Derived from UAV-Based RGB Imaging. *Remote Sensing*, *6*(11), 10395–10412. doi:10.3390/rs61110395

Bendig, J. V. (2015). *Unmanned aerial vehicles (UAVs) for multi-temporal crop surface modelling. A new method for plant height and biomass estimation based on RGB imaging* (Doctoral Thesis). University of Cologne, Faculty of Mathematics and Natural Sciences, Cologne.

Bendig, J., Yu, K., Aasen, H., Bolten, A., Bennertz, S., Broscheit, J., et al. (2015). Combining UAV-based plant height from crop surface models, visible, and near infrared vegetation indices for biomass monitoring in barley. *International Journal of Applied Earth Observation and Geoinformation*, *39*, 79–87. doi:10.1016/j.jag.2015.02.012

Castaldi, F., Pelosi, F., Pascucci, S., & Casa, R. (2017). Assessing the potential of images from unmanned aerial vehicles (UAV) to support herbicide patch spraying in maize. *Precision Agriculture*, *18*(1), 76–94. doi:10.1007/s11119-016-9468-3

Catchpole, W. R., & Wheeler, C. J. (1992). Estimating plant biomass: A review of techniques. *Australian Journal of Ecology*, *17*(2), 121–131. doi:10.1111/j.1442-9993.1992.tb00790.x

Chang, A., Jung, J., Maeda, M. M., & Landivar, J. (2017). Crop height monitoring with digital imagery from Unmanned Aerial System (UAS). *Computers and Electronics in Agriculture*, *141*, 232–237. doi:10.1016/j.compag.2017.07.008

Duan, T., Chapman, S. C., Guo, Y., & Zheng, B. (2017). Dynamic monitoring of NDVI in wheat agronomy and breeding trials using an unmanned aerial vehicle. *Field Crops Research*, *210*, 71–80. doi:10.1016/j.fcr.2017.05.025

Eisenbeiss, H. (2009). *UAV photogrammetry* (Doctoral Thesis). ETH Zurich, Switzerland.

Eitel, J. U. H., Höfle, B., Vierling, L. A., Abellán, A., Asner, G. P., Deems, J. S., et al. (2016). Beyond 3-D: The new spectrum of lidar applications for earth and ecological sciences. *Remote Sensing of Environment*, *186*, 372–392. doi:10.1016/j.rse.2016.08.018

Ganguli, A. C., Vermeire, L. T., Mitchell, R. B., & Wallace, M. C. (2000). Comparison of Four Nondestructive Techniques for Estimating Standing Crop in Shortgrass Plains. *Agronomy Journal*, *92*(6), 1211–1215. doi:10.2134/agronj2000.9261211x

Godwin, R. J., & Miller, P. C. H. (2003). A Review of the Technologies for Mapping Within-field Variability. *Biosystems Engineering*, *84*(4), 393–407. doi:10.1016/S1537-5110(02)00283-0

Hassan, M. A., Yang, M., Fu, L., Rasheed, A., Zheng, B., Xia, X., et al. (2019). Accuracy assessment of plant height using an unmanned aerial vehicle for quantitative genomic analysis in bread wheat. *Plant Methods*, *15*, 37. doi:10.1186/s13007-019-0419-7

Hoffmeister, D., Bolten, A., Curdt, C., Waldhoff, G., & Bareth, G. (2010). High-resolution Crop Surface Models (CSM) and Crop Volume Models (CVM) on field level by terrestrial laser scanning. In *Proc. SPIE 7840, Sixth International Symposium on Digital Earth: Models, Algorithms, and Virtual Reality* (Vol. 7840, p. 78400E). SPIE (Bellingham, USA). doi:10.1117/12.872315

Holman, F. H., Riche, A. B., Michalski, A., Castle, M., Wooster, M. J., & Hawkesford, M. J. (2016). High Throughput Field Phenotyping of Wheat Plant Height and Growth Rate in Field Plot Trials Using UAV Based Remote Sensing. *Remote Sensing*, *8*(12), 1031. doi:10.3390/rs8121031

Hugenholtz, C. H., Whitehead, K., Brown, O. W., Barchyn, T. E., Moorman, B. J., LeClair, A., et al. (2013). Geomorphological mapping with a small unmanned aircraft system (sUAS): Feature detection and accuracy assessment of a photogrammetrically-derived digital terrain model. *Geomorphology*, *194*, 16–24. doi:10.1016/j.geomorph.2013.03.023

Hunt, E. R., Hively, W. D., Fujikawa, S. J., Linden, D. S., Daughtry, C. S. T., & McCarty, G. W. (2010). Acquisition of NIR-Green-Blue Digital Photographs from Unmanned Aircraft for Crop Monitoring. *Remote Sensing*, *2*(1), 290–305. doi:10.3390/rs2010290

IGN. (2016). Caméra légère IGN | IGN Lightweight Camera. http://www.ign.fr/institut/innovation/camera-legere-ign. Accessed 8 October 2020

Inrae. (2019). QualiAgro. http://www6.inra.fr/qualiagro_eng. Accessed 8 October 2020

Johnson, L. F., Herwitz, S., Dunagan, S., Lobitz, B., Sullivan, D., & Slye, R. (2003). Collection of Ultra High Spatial and Spectral Resolution Image Data over California Vineyards with a Small UAV. In

Proceedings of the 30th International Symposium on Remote Sensing of Environment (pp. 10–14). ICRSE (Columbia, USA).
Kraus, K., & Waldhäusl, P. (1998). *Manuel de photogrammétrie: Principes et procédés fondamentaux (Photogrammetry Manual: Basic Principles and Processes)*. Hermès (Paris, France).
Li, W., Niu, Z., Chen, H., Li, D., Wu, M., & Zhao, W. (2016). Remote estimation of canopy height and aboveground biomass of maize using high-resolution stereo images from a low-cost unmanned aerial vehicle system. *Ecological Indicators*, *67*, 637–648. doi:10.1016/j.ecolind.2016.03.036
Lindblom, J., Lundström, C., Ljung, M., & Jonsson, A. (2017). Promoting sustainable intensification in precision agriculture: review of decision support systems development and strategies. *Precision Agriculture*, *18*(3), 309–331. doi:10.1007/s11119-016-9491-4
Liu, S., Baret, F., Abichou, M., Boudon, F., Thomas, S., Zhao, K., et al. (2017). Estimating wheat green area index from ground-based LiDAR measurement using a 3D canopy structure model. *Agricultural and Forest Meteorology*, *247*, 12–20. doi:10.1016/j.agrformet.2017.07.007
Lowe, D. G. (2004). Distinctive Image Features from Scale-Invariant Keypoints. *International Journal of Computer Vision*, *60*(2), 91–110. doi:10.1023/B:VISI.0000029664.99615.94
Mulla, D. J. (2013). Twenty five years of remote sensing in precision agriculture: Key advances and remaining knowledge gaps. *Biosystems Engineering*, *114*(4), 358–371. doi:10.1016/j.biosystemseng.2012.08.009
Noirot-Cosson, P. E., Vaudour, E., Gilliot, J. M., Gabrielle, B., & Houot, S. (2016). Modelling the long-term effect of urban waste compost applications on carbon and nitrogen dynamics in temperate cropland. *Soil Biology and Biochemistry*, *94*, 138–153. doi:10.1016/j.soilbio.2015.11.014
Phase one. (2018). Phase One IXM cameras. *industrial.phaseone.com*. https://industrial.phaseone.com/iXM_Camera_Series.aspx. Accessed 8 October 2020
Pinter, Jr., P. J., Hatfield, J. L., Schepers, J. S., Barnes, E. M., Moran, M. S., Daughtry, C. S. T., et al. (2003). Remote Sensing for Crop Management. *Photogrammetric Engineering & Remote Sensing*, *69*(6), 647–664. doi:10.14358/PERS.69.6.647
Poblete-Echeverría, C., Olmedo, G. F., Ingram, B., & Bardeen, M. (2017). Detection and Segmentation of Vine Canopy in Ultra-High Spatial Resolution RGB Imagery Obtained from Unmanned Aerial Vehicle (UAV): A Case Study in a Commercial Vineyard. *Remote Sensing*, *9*(3), 268. doi:10.3390/rs9030268
R Development Core Team. (2016). R: The R Project for Statistical Computing. https://www.r-project.org/. Accessed 8 October 2020
senseFly - eMotion. (n.d.). *senseFly*. https://www.sensefly.com/software/emotion. Accessed 16 June 2020
Sun, S., Li, C., & Paterson, A. H. (2017). In-Field High-Throughput Phenotyping of Cotton Plant Height Using LiDAR. *Remote Sensing*, *9*(4), 377. doi:10.3390/rs9040377
Ullman, S. (1979). The Interpretation of Structure from Motion. *Proceedings of the Royal Society of London. Series B. Biological Sciences*, *203*(1153), 405–426. doi:10.1098/rspb.1979.0006
Verger, A., Vigneau, N., Chéron, C., Gilliot, J. M., Comar, A., & Baret, F. (2014). Green area index from an unmanned aerial system over wheat and rapeseed crops. *Remote Sensing of Environment*, *152*, 654–664. doi:10.1016/j.rse.2014.06.006
Wood, S. (2017). https://cran.r-project.org/web/packages/mgcv/mgcv.pdf. *Package 'mgcv.'*
Yue, J., Yang, G., Li, C., Li, Z., Wang, Y., Feng, H., et al. (2017). Estimation of Winter Wheat Above-Ground Biomass Using Unmanned Aerial Vehicle-Based Snapshot Hyperspectral Sensor and Crop Height Improved Models. *Remote Sensing*, *9*(7), 708. doi:10.3390/rs9070708
Zhang, C., & Kovacs, J. M. (2012). The application of small unmanned aerial systems for precision agriculture: a review. *Precision Agriculture*, *13*(6), 693–712. doi:10.1007/s11119-012-9274-5
Zhang, N., Wang, M., & Wang, N. (2002). Precision agriculture—a worldwide overview. *Computers and Electronics in Agriculture*, *36*(2), 113–132. doi:10.1016/S0168-1699(02)00096-0
Zhou, X., Zheng, H. B., Xu, X. Q., He, J. Y., Ge, X. K., Yao, X., et al. (2017). Predicting grain yield in rice using multi-temporal vegetation indices from UAV-based multispectral and digital imagery. *ISPRS Journal of Photogrammetry and Remote Sensing*, *130*, 246–255. doi:10.1016/j.isprsjprs.2017.05.003